AD-A157 133 EFFECT OF GRAIN BOUNDARY STRUCTURE ON SENSITIZATION AND CORROSION OF STAI.. (U) PENNSYLVANIA STATE UNIV UNIVERSITY PARK DEPT OF MATERIALS SCI.. 1/1

UNCLASSIFIED B W BENNETT ET AL. JUN 85 N00014-81-K-0025 F/G 11/6 NL

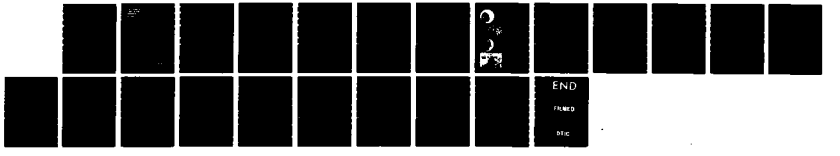

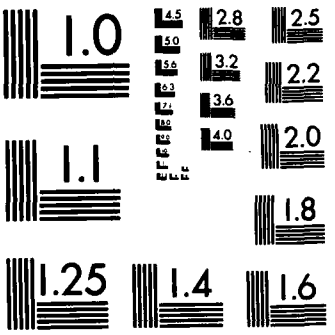

MICROCOPY RESOLUTION TEST CHART

ANNUAL TECHNICAL REPORT

June 1985

OFFICE OF NAVAL RESEARCH

Contract No. N000-14-81-K-0025

EFFECT OF GRAIN BOUNDARY STRUCTURE ON SENSITIZATION AND CORROSION OF STAINLESS STEEL

B. W. Bennett and H. W. Pickering

Department of Materials Science and Engineering
The Pennsylvania State University
University Park, Pennsylvania 16802

The Pennsylvania State University

University Park, Pennsylvania

THE PENNSYLVANIA STATE UNIVERSITY

College of Earth and Mineral Sciences

UNDERGRADUATE PROGRAMS OF STUDY

Ceramic Science and Engineering, Earth Sciences, Fuel Science, Geography, Geosciences, Metallurgy, Meteorology, Mineral Economics, Mining Engineering, Petroleum and Natural Gas Engineering, and Polymer Science.

GRADUATE PROGRAMS AND FIELDS OF RESEARCH

Ceramic Science, Fuel Science, Geochemistry and Mineralogy, Geography, Geology, Geophysics, Metallurgy, Meteorology, Mineral Economics, Mineral Processing, Mining Engineering, Petroleum and Natural Gas Engineering, and Polymer Science.

UNIVERSITY-WIDE INTERDISCIPLINARY GRADUATE PROGRAMS INVOLVING E&MS FACULTY AND STUDENTS

Earth Sciences, Ecology, Environmental Pollution Control Engineering, Mineral Engineering Management, Operations Research, Regional Planning, and Solid State Science.

ASSOCIATE DEGREE PROGRAMS

Metallurgical Engineering Technology and Mining Technology.

INTERDISCIPLINARY RESEARCH GROUPS WITHIN THE COLLEGE

Coal Research Section, Mineral Conservation Section, Ore Deposits Research Section, and Mining and Mineral Resources Research Institute.

ANALYTICAL AND STRUCTURE STUDIES

Classical chemical analysis of metals and silicate and carbonate rocks; X-ray crystallography; electron microscopy and diffraction; electron microprobe analysis; atomic absorption analysis; spectrochemical analysis.

U.Ed. 9-725

SECURITY CLASSIFICATION OF THIS PAGE (When Data Entered)

REPORT DOCUMENTATION PAGE		READ INSTRUCTIONS BEFORE COMPLETING FORM
1. REPORT NUMBER Annual Technical Report	2. GOVT ACCESSION NO. AD-A157 133	3. RECIPIENT'S CATALOG NUMBER
4. TITLE (and Subtitle) EFFECT OF GRAIN BOUNDARY STRUCTURE ON SENSITIZATION AND CORROSION OF STAINLESS STEEL		5. TYPE OF REPORT & PERIOD COVERED Annual Technical Report 6. PERFORMING ORG. REPORT NUMBER
7. AUTHOR(s) B. W. Bennett and H. W. Pickering		8. CONTRACT OR GRANT NUMBER(s)
9. PERFORMING ORGANIZATION NAME AND ADDRESS Metallurgy Program, 209 Steidle Building The Pennsylvania State University University Park, PA 16802		10. PROGRAM ELEMENT, PROJECT, TASK AREA & WORK UNIT NUMBERS
11. CONTROLLING OFFICE NAME AND ADDRESS Metallurgy Branch Office of Naval Research Arlington, VA 22217		12. REPORT DATE June, 1985 13. NUMBER OF PAGES
14. MONITORING AGENCY NAME & ADDRESS(if different from Controlling Office)		15. SECURITY CLASS. (of this report) 15a. DECLASSIFICATION/DOWNGRADING SCHEDULE
16. DISTRIBUTION STATEMENT (of this Report)		
17. DISTRIBUTION STATEMENT (of the abstract entered in Block 20, if different from Report)		
18. SUPPLEMENTARY NOTES		
19. KEY WORDS (Continue on reverse side if necessary and identify by block number)		

20. ABSTRACT (Continue on reverse side if necessary and identify by block number)

This paper reports on a study of intergranular corrosion, particularly the influence of the crystallography of a grain boundary (g.b.) on the sensitization and grain boundary corrosion of stainless steels. Since sensitization of stainless steels depends on g.b. energy, this study included a determination of the misorientation angle of grain boundaries in a sample. A scanning electron microscope was modified for application of the electron backscattering (EBS) technique in conjunction with normal SEM imaging of the

DD FORM 1 JAN 73 1473 EDITION OF 1 NOV 65 IS OBSOLETE
S/N 0102-014-6601

SECURITY CLASSIFICATION OF THIS PAGE (When Data Entered)

sample surface. Using the EBS technique the orientations of neighboring grains were readily obtained with an accuracy of $\pm$ 0.5°.

In austenitic stainless steel (Fe-18Cr-10Ni) samples annealed at 1200°C for 1 hr., water quenched and aged for various times at 650°C, the degree of sensitization increased with increasing aging time. This was indicated by an increasing width of the g.b. groove. A plot of groove width vs. g.b. misorientation angle obtained by the EBS technique showed a range of groove widths for the same angle. Modeling the g.b. structure based on ideal crystallography and the coincident site lattice concept provided a rationalization of this observation. Similar results were found for ferritic stainless steel (Fe-19 Cr) samples.

The Cr concentration profiles as a function of time were calculated, using a finite difference method, both along the g.b. and normal to the g.b. These profiles agree well with Cr profiles experimentally measured by other investigators. The calculation includes overlap of the chromium profiles in the boundary, and considers the dependence of sensitization on aging time, g.b. diffusivity, carbide spacing and g.b. width.

A major difficulty in understanding g.b. corrosion is the difference in the groove and Cr-profile widths. The observed groove widths are 10 to 100 times larger than the Cr-profile widths.

Introduction

This paper summarizes our progress to date on one of two thrusts of our current Office of Naval Research grant on grain boundary corrosion: The effect of grain boundary structure on the sensitization of stainless steels (1). The other thrust concerns the characterization and mechanism of the electrochemical process which occurs in the grain boundary groove, and more generally in all localized cell corrosion.

Many examples of uneven attack at grain boundaries of a sample are available in the literature. The energy associated with grain boundaries makes them favorable sites for solute segregation. precipitation and electrochemical reactions, one or all of which can lead to corrosion at the grain boundary. Grain boundary energy is a function of g.b. structure and, therefore, varies among the boundaries of a sample. This can cause variations in the extent of any or all of these processes at the grain boundaries.

Many theoretical models and calculations in the literature consider the relationship of the grain boundary structure and grain boundary energy. Notable among them are the dislocation models proposed by Burger (2), Bragg (3) and Read and Shockley (4). Cusps of lower grain boundary energy were predicted in the energy vs. misorientation angle at intermediate values of grain boundary misorientation (4). These cusps have been rationalized on the basis of the coincident site lattice (CSL) model advanced by Bollman (5). Coincident sites are those where atoms of the adjacent grains forming the grain boundary exactly register or coincide. Low energy cusps occur when coincidence occurs on the same atom at regular intervals of small (atomic) spacing. An increase in grain boundary energy is associated with both a deviation from a CSL orientation and a closer spacing of associated secondary grain boundary dislocations. Atomistic calculations can lead to the cusped nature of the grain boundary energy with misorientation, such as those performed by Sutton and Vitek (6).

Calculations have also been made on the solute redistribution associated with segregation or precipitation at a grain boundary. For example, a more quantitative understanding of grain boundary corrosion of stainless steel is obtained from the chromium depletion models proposed by Stawstrom and Hillert (7), Tedmon et. al. (8) and Hall and Briant (9). These models, however, do contain somewhat arbitrary assumptions, e.g., 20 nm for the minimum width of the Cr-depleted region (7). Because of these and other assumptions, existing models are deficient, e.g., they do not adequately model the sensitization process when chromium profiles in the boundary overlap.

This paper describes a study of the relationship of grain boundary structure to the extent of the sensitization process in stainless steels. For determination of grain boundary structure it was necessary to determine the orientations of the adjacent grains. This paper also describes a more complete kinetic model of the sensitization process.

Ideally, atom probe field ion microscopy would serve to determine orientation, grain boundary structure, precipitation of carbides and chromium depletion. Specimen preparation is difficult since it requires a grain boundary in the field of APFIM, although some encouraging progress has been made in the in-situ formation of grain boundaries in the APFIM using a laser (10). Electron channelling patterns are widely used for such purposes but not all scanning electron microscopes (SEM) can be used in this way. On the other hand the electron back scattering (EBS) technique can be used with virtually all scanning electron microscopes for the determination of crystal orientation (11-14).

Experimental

The EBS technique, originally developed by German researchers (11,12), can be operated with an SEM using a stationary electron beam at currents of 10^{-8} to 10^{-7} A (13,14). The incident electrons are inelastically scattered by the sample and then elastically backscattered (Bragg reflected). In order to sense these Bragg reflected electrons the sample is tilted between 60 and 85°, enabling the backscattered electrons to impinge on a phosphor screen. An SEM micrograph is taken in this position for grain identification. The patterns obtained on the phosphor screen are viewed and photographed through a glass window that is inserted in an unused port of the SEM sample chamber.

The patterns produced on the screen conform to stereographic projections of the planes of the crystal, thereby enabling both the orientation (to ± 0.5°) and structure of the crystal to be determined. In addition, the good spacial resolution enables grains as small as a few m in a polycrystalline sample to be analyzed. The quality of EBS patterns depends strongly on the surface condition, degrading as reaction-product layers accumulate on the surface.

The patterns obtained from the two phases in a dual phase CD-4MCu alloy are shown in Figure 1. The analyses of these patterns, representing a grain of each phase, austenitic above and ferritic below the micrograph, provides the orientations of the two grains and the structures of the two phases. As a result of the wide angle of coverage, most EBS patterns can be readily indexed by simply noting the major symmetry elements in the patterns. In the upper left pattern of Figure 1, the two-fold symmetry elements about the <110> pole are apparent. The completely indexed pattern appears on the right, where major poles are labelled within the circle and the planes responsible for producing the respective bands are labelled outside of the circle. Other aids, in the indexing and structure determination, are the obvious presence or absence of major poles and the relative widths of bands in the pattern: both are consequences of Bragg reflection. Only for planes satisfying the appropriate structure factor conditions, for the particular crystal system, will EBS bands be formed*. As with Kikuchi or electron channelling bands, widths of EBS bands are proportional to 2 sin θ where θ is the Bragg angle. It follows that the planes having low indices produce narrow and well defined EBS bands. Further details on the EBS technique and its application in this study can be found elsewhere (14).

To establish grain boundary structure, orientation information obtained with the EBS technique was combined with the observation that grain boundaries are often near normal to the sample surface. Therefore, in analyses of the ideal (unrelaxed) grain boundary structure the boundaries were assumed to be perpendicular to the sample surface. The resulting boundary structure was plotted with a Houston Instruments DMP-29 plotter interfaced to a Commodore 64 microcomputer. Plots consist of overlays of the ideal atomic arrangements in the boundary plane of both crystals. Angle axis pairs were also calculated (15) and by manipulating the rotation matrix used in the calculation so as to maximize the diagonal terms, the minimum rotation (misorientation) angle was determined.

The effect of crystallography on grain boundary corrosion was studied in an austenitic Fe-18Cr-10Ni and a ferritic Fe-19Cr stainless steels. Their

*Note the prominence of the 211 pole in the EBS pattern of the austenitic phase, formed by the intersection of the $\bar{1}11$ and $0\bar{2}2$ bands. The pattern from the ferritic phase, however, prominently displays a 311 pole formed by the intersection of the $\bar{1}12$, $\bar{1}21$ and $01\bar{1}$ bands.

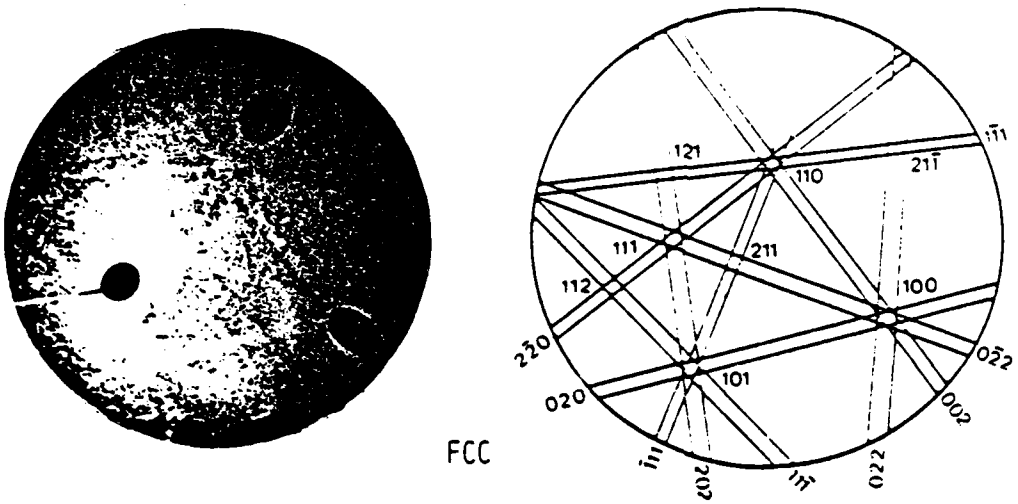

Fig. 1. SEM micrograph and EBS patterns of a dual phase alloy, ferrite matrix and second phase austenite, CD-4MCu alloy (14).

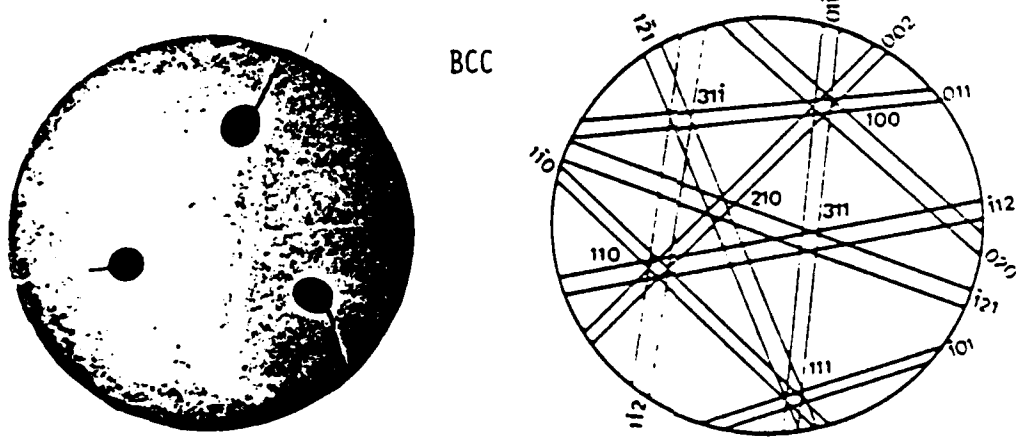

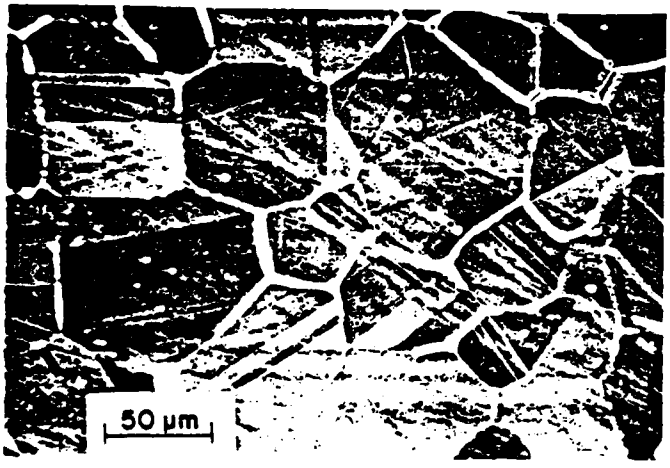

Figure 2. SEM micrograph of austenitic stainless steel aged 1 hr at 650°C, and exposed to 1 N H_2SO_4 at 0.34 V (SHE).

compositions are given in Table 1. Following rolling to 500 μm, 0.5 x 1 cm^2 samples of Fe-18Cr-10Ni were cut, mechanically polished, cleaned ultrasonically, individually vacuum encapsulated in Vycor after purging with high purity argon and annealed at 1200°C for 1 hr and water quenched. Subsequently, the Fe-18Cr-10Ni samples were isothermally aged at 650°C for 1, 10, 100 or 1000 hr. The ferritic Fe-19Cr samples were prepared similarly after rolling to 1000 m and prepared as above except that the samples were either water quenched or air cooled from the 1200°C anneal and not aged.

Table 1. Compositions of Stainless Steels

Alloy	Cr	Ni	C	S	P	BAL
Fe-18Cr-10Ni	17.82	9.88	0.11	0.02	0.02	Fe
Fe-19Cr	19.47	-	0.09	0.02	0.02	Fe

Final grain sizes of both stainless steel samples varied from 10 to 250 m. The austenitic samples were heavily twinned. The austenitic and ferritic samples were then mechanically polished through 0.05 μm alumina. Some of these samples were electropolished in a 7% perchloric acid, 90% (glacial) acetic acid, 3% H_2O solution at 21 V for 30 to 60 s to remove the deformation layer in preparation for the EBS analysis.

The widths of the grooves that formed along the grain boundaries during anodic polarization were measured. The average values were used to represent the extent of corrosion at the different grain boundaries of the sample.

A three electrode closed cell was used to anodically polarize the samples. Saturated calomel and Pt cyclindrical mesh electrodes were used as the reference and counter electrodes, respectively. The electrolyte was 1N H_2SO_4 prepared from reagent grade sulfuric acid and doubly distilled water and deaerated with oxygen-free argon. The temperature of the solution was 21 ± 2°C. Electrode potentials are reported on the standard hydrogen scale.

After introducing the sample, the cell was allowed to stabilize until the corrosion potential approached a nearly constant value, typically after 10 minutes. Constant potentials of 340 and 140 mV (SHE) for the austenitic and ferritic samples, respectively, were used based on numerous trials which showed these potentials provided the greatest degree of intergranular attack in sensitized samples. Both alloys are passivated at these potentials in the nonsensitized condition. The time of these constant potential exposures ranged from 300 to 1800 s. The samples were then analyzed by light and scanning electron microscopy and the EBS technique.

The finite difference calculations of the diffusion profiles in, and normal to, the grain boundary required a large number of operations to perform an adequate simulation, and were accomplished using a high speed IBM 4381 computer. Typically, for an adequate simulation of a one hour sensitization process, computer execution times would range from approximately 10 to 15 minutes.

Results

Austenitic Stainless Steel

The anodic polarization curves for the Fe-18Cr-10Ni samples, annealed and isothermally aged at 650°C for various times, show that with increasing aging

time, the active-passive transition occurs at more oxidizing potentials and the passive current density increases. Similarly aged Fe-18Cr-10Ni samples were polarized at 340 mV (SHE) for 5 min and examined by SEM. Strong grain boundary corrosion occurred in contrast to unsensitized samples which showed no grain boundary attack. With increasing aging times, the degree of grain boundary corrosion increased, as indicated from the measured groove widths, approximately 0.5 to 1 μm and 2 to 3 μm for 1 and 1000 hr at 650°C, respectively. After 1 hr aging at 650°C, several grain boundaries were strongly attacked during polarization, whereas others remained intact, Figure 2. Coherent twin boundaries also showed no sign of dissolution for the samples that were polarized after aging for 1 hr at 650°C. With increasing aging time, the extent and density of corroded grain boundaries increased. After 100 hr of aging, grain interiors also exhibited substantial localized attack, and the severely grooved grain boundaries revealed a continuous grain boundary phase, presumably $M_{23}C_6$. The continuity of this phase was even more visible after 1000 hr of aging, since it stood in relief along all of the grain boundaries. The plate-like precipitate was oriented, for the most part, normal to the sample surface. After 1000 hr of aging, the coherent twin boundaries were also heavily attacked and, in addition, contained a narrower groove centered along the major groove bottom. This narrower groove was visible because carbides were not present in the twin boundaries in contrast to their strong prominence along all of the grain boundaries.

Because one hour at 650°C produced the greatest variation in sensitization of the boundaries, EBS pattern were obtained for the grains in Figure 2, and analysed for misorientation angle and ideal (unrelaxed) atomic structure of the boundaries. The misorientation angles varied over a wide range with a larger than random number of low angle boundaries. The groove width was not simply related to misorientation angle, e.g., a wide range of groove widths occurred for the same 14° angle, and there was no apparent relationship between groove width and misorientation angle.

Boundaries with similar misorientation angle, that exhibited different corrosion behavior after 1 hr aging at 650°C, were examined in more detail. In the several boundaries examined, it was apparent that the underlying factor determining the degree of sensitization and grooving was the coincidence of the atomic positions of the two lattices at the boundary. Coincidence was found to be relatively low for heavily grooved boundaries and relatively high for lightly grooved boundaries of the same misorientation. A particularly striking example of a nearly perfect coincidence and a quite low coincidence is shown in Figure 3 for the ferritic stainless steel.

Ferritic Stainless Steel

A variable amount of grain boundary attack was also observed in the Fe-19Cr alloy, anodically polarized following a quench from the 1200°C annealing temperature. EBS patterns from the individual grains were obtained, and the grain boundary atomic structures were determined. A relationship between misorientation angle and grain boundary groove width was observed as shown in Figure 4, in contrast to the absence of a relationship in the austenitic samples. Atomic structures of a single boundary, which was heavily grooved over one segment and lightly grooved over another segment, are shown in Figure 3. The misorientation angle, between the adjacent grains in Figure 3, is 9°.

Finite Difference Model of Sensitization

By employing finite difference calculations, a kinetic model of sensitization was developed for stainless steel. It overcomes many of the

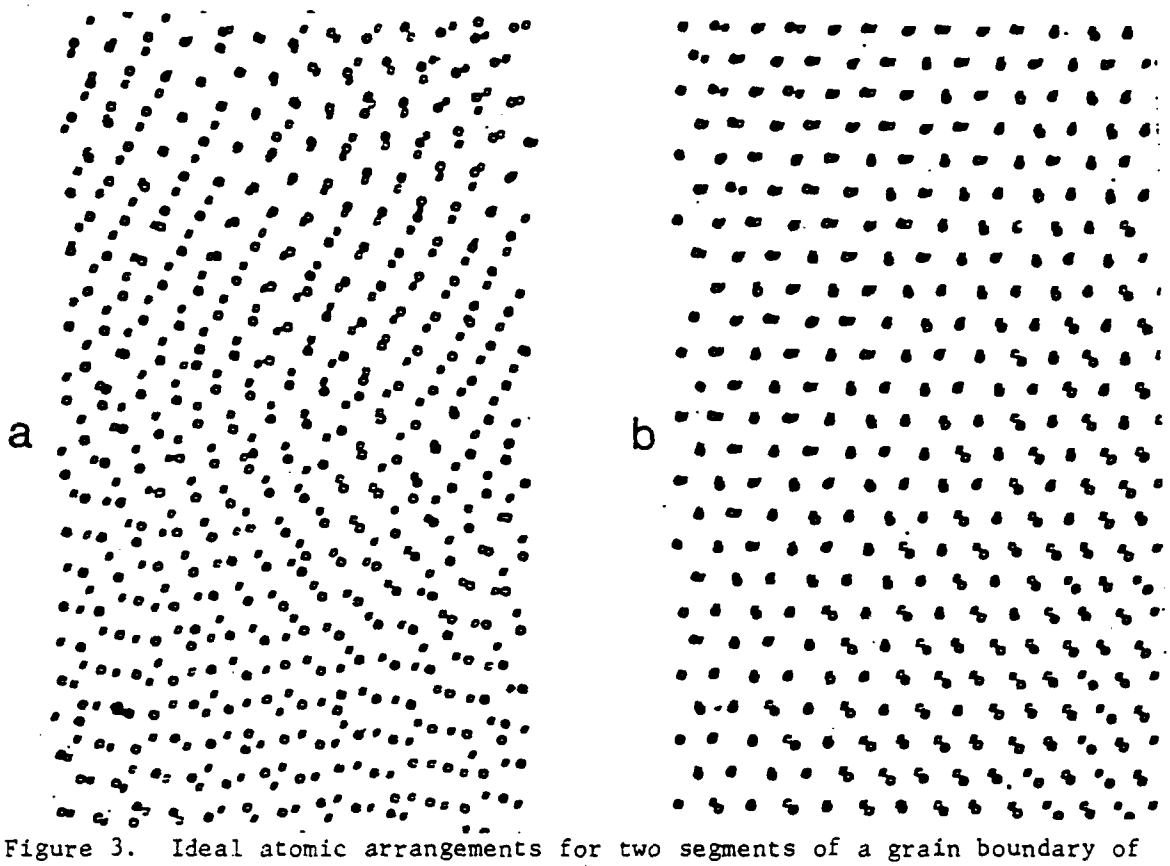

Figure 3. Ideal atomic arrangements for two segments of a grain boundary of 9° misorientation angle. (a) heavily grooved segment, (b) lightly grooved segment.

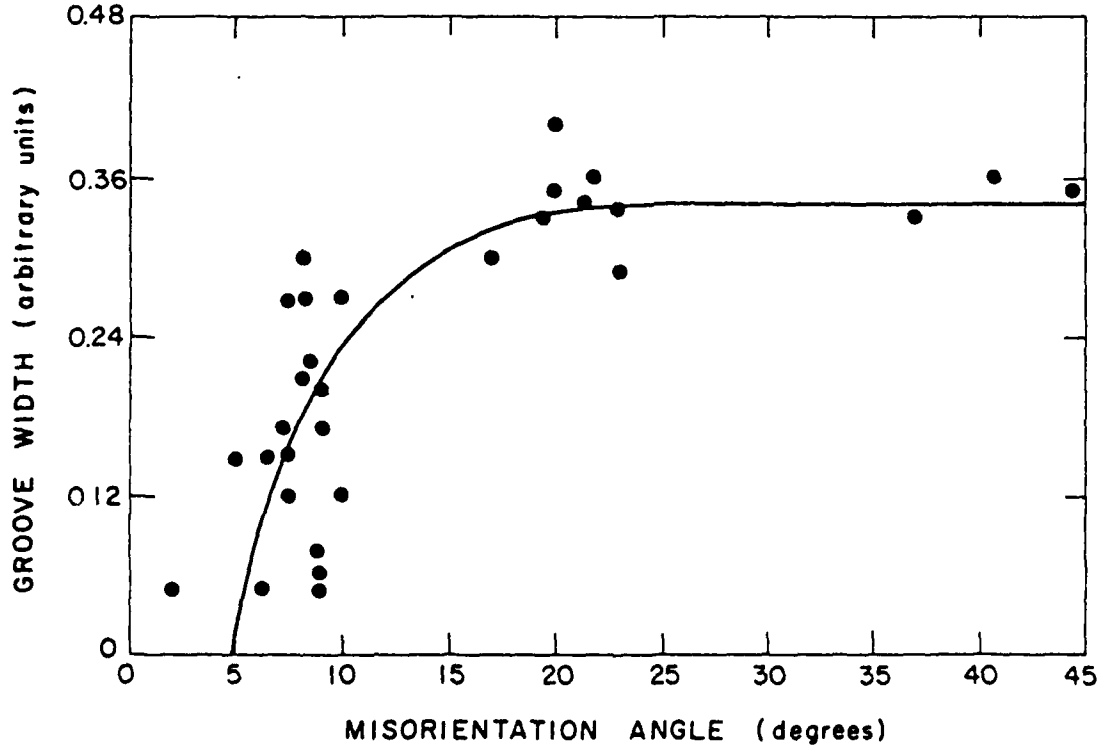

Figure 4. Grain boundary groove width as a function of misorientation angle for a sample of the ferritic stainless steel.

limitations associated with earlier models. The phenomenological approach, assumptions, results and conclusions will be presented here.

The physical model consists of the growth of two parallel lath-like grain boundary precipitates, in which both the grain boundary and the volume diffusion play a role. Grain boundary diffusion produces a composition profile in the boundary. Volume diffusion produces profiles normal to the boundary. One way to envision the model is to consider a fast, but narrow diffusing grain boundary region bordered by a slowly leaking bulk phase. This is essentially the basis of the "collector plate" model, proposed by Aaron and Aaronson (16). For the particular case of sensitization, the model also considers that a boundary is sensitized when the chromium concentration throughout the boundary falls below 13 at %.

In developing the finite difference equation for the grain boundary concentration profiles, it is assumed that

1. Volume diffusion only occurs normal to the boundary.

2. The boundary composition is constant in the thickness direction, i.e., no y direction profile in the boundary.

3. Carbide growth is slow enough so that the carbide matrix interface remains essentially stationary.

Some additional assumptions are the same as needed for the simpler one-dimensional diffusion problem.

The finite difference calculation of diffusion profiles in, and normal to, the grain boundary is a two-step process for each iteration. First, the chromium concentration profile in the boundary after an increment of time Δt is calculated. For the first iteration, all values are equal to the bulk Cr concentration, except for the boundary concentration at the carbide surface. The latter is the chromium concentration in the matrix in equilibrium with the $Cr_{23}C_6$ carbide at the matrix-carbide interface. After completion of the calculation of the Cr concentration profile in the boundary, Cr profiles are calculated normal to the boundary. This completes one iteration of the calculation. The process is repeated $t_s/\Delta t$ times, where t_s equals the total simulation time of diffusion.

Since the model includes sensitization time and temperature, precipitate spacing, grain boundary and volume diffusivity, and grain boundary width as parameters, it provides a powerful means to theoretically investigate the sensitization process with a strong emphasis on the effect of grain boundary structure.

Sensitization time as a variable is illustrated for an austenitic stainless steel containing 18 Cr is shown in Figure 5. The profiles in the boundary (x direction) and normal to the boundary into one of the adjacent grains (y direction) are shown. The dashed line in the grain boundary plane represents the 13 at% Cr level. For the calculation, a temperature of 650°C was chosen because it is near the "knee" of the time-temperature-sensitization curve (17). The corresponding grain boundary and volume diffusivities for the austenitic stainless steel are $D_{gb} = 10^{-11}$ cm^2 s^{-1} and $D_{vol} = 10^{-16}$ cm^2 s^{-1} (18). The matrix composition in equilibrium with the carbide precipitate was taken as 10 at.%. Grain boundary width was set at $\delta = 10^{-7}$ cm, and carbide spacing was set at 1.02 μm based on a measured average carbide spacing of ~1μm for austenitic stainless steels sensitized near this temperature (19). The calculation was done for sensitization times of 1, 10, 100, 1000 and 10,000 s.

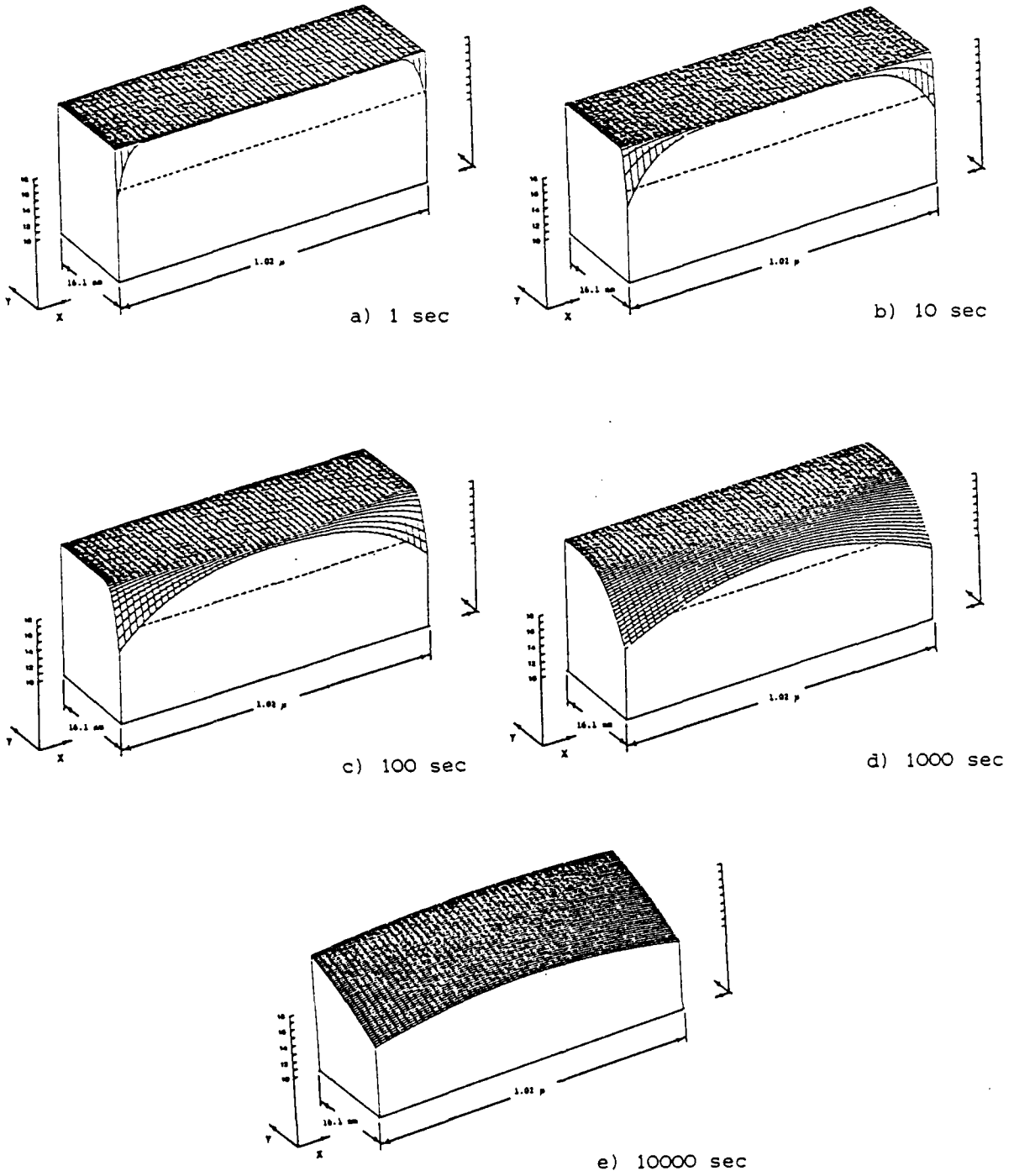

Figure 5. Calculated Cr concentration profiles in the boundary (x direction) and normal to the boundary into one of the adjacent grains (y) for a carbide spacing of 1.02 μm in austenitic stainless steel aged at 650°C for various times. Cr concentration is plotted along the vertical axis (z direction).

After 1 s, a profile in the grain boundary is already forming while the concentration normal to the boundary remains essentially constant (Figure 5a). After 10 s, the boundary profiles are more developed but still not overlapping and the profiles normal to the boundary are just becoming noticeable. Overlapping of the profile in the boundary plane appears after approximately 100 s. After 1000 s, overlapping is extensive and over one-quarter of the boundary (near the carbides) has less than 13% Cr and the profiles normal to the boundary are also well developed. The profile normal to the boundary, however, is still quite shallow ($\sim 10^{-6}$ cm). At 2290 s (~50 min), the Cr concentration is below 13 at % Cr at all points in the grain boundary, in agreement with most experimental results that indicate sensitization at 650°C occurs in approximately 1 hr.

Several parameters can be varied in the model. Carbide spacing as a variable was illustrated, by comparing results for a spacing of 0.5×10^{-4} cm with the above results for 1.0×10^{-4} cm, keeping all other values the same. A marked difference was apparent once overlap of the profiles occurred in the boundary. Overlap occurs after only 10 s for the 0.5 μm spacing, whereas it does not occur in that time for the 1 μm spacing (Figure 5b) i.e. with the narrower precipitate spacing, the chromium concentration is lower in the boundary plane. In contrast, overlap does not occur for either spacing after 1 s and accordingly, the calculated profiles are identical. As time at 650°C increases to 100 s, the difference in Cr level in the boundary for the two carbide spacings increases and is still large at 1000 s. Furthermore, by 1000 s the chromium concentration falls below 13 at.% along the entire boundary for the narrower spacing, in contrast to the situation for the larger spacing (Figure 5d). With further increase in time, the difference in Cr level in the boundary for the two spacings begins to decrease and eventually vanishes as the Cr concentration falls to the equilibrium value (~10 at.%) everywhere in the boundary. At this time the Cr concentration for the two spacings normal to the boundary also approach the same profile, expectantly an "erf" type profile in accord with a uniform boundary composition.

For ferritic stainless steels sensitization occurs relatively quickly, typically within the period of a quench from a high temperature anneal. This is consistent with a volume diffusivity of chromium that is almost two orders of magnitude greater in ferritic than in austenitic stainless steel (20), as well as a higher interstitial diffusion. A higher diffusivity in the ferritic phase, coupled with little difference in the grain boundary diffusivities (18), provides for a smaller carbide spacing for the ferritic than the austenitic stainless steel. As a first approximation for application of the finite difference model to ferritic stainless steel, carbide spacing and sensitization temperature were assumed to be 5×10^{-6} cm and 550°C, respectively. At 550°C, D_{gb} and D_{vol} were calculated to be approximately 1×10^{-12} and 3×10^{-15} $cm^2 s^{-1}$, respectively. The bulk concentration was set at 18 at % Cr, and the equilibrium carbide-matrix composition was assumed to be 10 at. % Cr. The grain boundary width was assumed to be 10^{-7} cm. The chromium profiles for 1, 10, 100 and 1000 s were calculated and appear reasonable based on continuous cooling results (21) but, unfortunately, no direct isothermal aging experimental results are available.

Calculations of the Cr profiles using the finite difference method were also done for the conditions of available experimental data in the literature. The finite difference calculations produced excellent agreement with the experimentally determined Cr profiles, in and normal to the grain boundary, by Hall and Briant (9).

Discussion

Effect of Grain Boundary Structure

In both the austenitic and the ferritic stainless steels, chromium carbide precipitation during heat treatment occurred to different extents among boundaries of the same sample. This was shown by different amounts of grooving among the boundaries. In the ferritic alloy the precipitation process is much faster, in accord with the higher bulk chromium and interstitual diffusivities in the matrix. As a result, precipitation in the ferritic alloy proceeds to the advanced stage of a continuous phase along grain boundaries during very brief excursions in the sensitization temperature range, e.g., during cooling from the 1200°C anneal. On the other hand, for the austenitic alloy, follow up isothermal aging for relatively long times is required to sensitize the grain boundaries. In this case a qualitative relation between the required aging time for sensitization and boundary energy is evident: the lower the boundary energy, the longer the aging time. Even the very low energy coherent twin boundaries are sensitized after 1000 hr at 650°C, although, apparently, they do not contain carbides in contrast to all of the grain boundaries which do. One explanation is that the energy of the coherent twin bundaries is so low that carbides do not nucleate. In this event sensitization of these boundaries would have had to occur by chromium diffusion along the twin boundaries to carbides in the adjacent grain boundaries.

The differences in the amount of corrosion among various grain boundaries in a sample were significant in both the ferritic and austenitic alloys. The total amount of carbide per unit length of grain boundary, nuclei density and growth rate are all expected to be strong functions of grain boundary structure which in turn depends on such parameters as the misorientation angle and the boundary plane orientation.

Misorientation angle was clearly found not to be sufficient by itself to determine the relative amounts of grain boundary grooving among the boundaries, particularly in the austenitic alloy where the carbide distribution along grain boundaries in the same sample ranged from small, widely spaced precipitates to a continuous phase. Misorientation angle however, provided more insight in the case of the ferritic alloy where, in contrast to the austenitic alloy, a relation between groove width and misorientation angle was observed (Figure 4). Boundaries, misoriented by less than 10 degrees, exhibited low degrees of corrosion. The number of grain boundaries with low misorientation angle was higher than that for a random distribution, in both the ferritic an austenitic alloys.

The sharp change in groove width with misorientation angle at approximately 8-10° in Figure 4 suggests that below this angular range little or no carbide formation occurs: whereas above this value carbides nucleate and grow with the total amount of carbide formed being nearly constant with misorientation angle above 10°. In the 8-10° angle range a wide spectrum of groove widths was observed, indicating that other parameters are required to describe the precipitation process in these boundaries. Analysis of the coincidence of atomic sites, at the grain boundary, of adjacent grains was helpful in this regard. In particular, a boundary with a misorientation angle of 9° provided a rare opportunity since one segment was heavily grooved while another segment was lightly grooved. The ideal atomic arrangements of these segments shown in Figs. 3a and 3b indicate that the heavily grooved segment has a low coincidence and, therefore, is of a high energy: whereas the lightly grooved segment has a high coincidence and is of low energy. These results are in accord with the expected behavior between the extent of the sensitization process and the boundary energy.

In the case of the austenitic stainless steel where no relation was apparent between groove width and misorientation angle over the entire angular range, it was again apparent from consideration of the atomic arrangements that the more heavily grooved boundaries were of lower coincidence and higher energy than the lightly grooved boundaries.

Corrosion Mechanism

Although the use of groove width as a relative measure of the extent of grain boundary carbide formation is largely born out by the results, groove width is not simply related to the chromium concentration profile. The latter conclusion is also apparent from micrographs in papers by Briant (22) and Streicher (23). The fact that groove width is one or even two orders of magnitude larger than the Cr profile normal to the boundary, indicates that the grain boundary dissolution process is more complicated than the simple dissolution of the Cr-depleted alloy. One possibility is that after dissolution of the Cr-depleted alloy, a localized corrosion condition develops. Stainless steel is susceptible to pitting and crevice corrosion at potentials in the passive region. The initial groove has the appropriate geometry and dimensions to function as a crevice. This, or some other two-step grain boundary corrosion process, is also indicated by the presence of a narrower groove at the bottom of the main groove of the coherent twin boundaries. The narrower groove could have formed by the dissolution of the Cr-depleted alloy.

Finite Difference Model

Of the several assumptions in the finite difference calculation, seemingly only in the case of the ferritic stainless steel is there some question. This concerns the assumption that the matrix/carbide interface is stationary. Because the carbides are so close together in the boundaries of the ferritic alloy, the actual motion of the boundaries becomes a significant fraction of the carbide spacing during the longer simulated aging times. Thus, for the ferritic stainless steels, a moving boundary calculation would give more realistic profiles. On the other hand, in the case of the austenitic stainless steels all of the assumptions seem well justified and this is borne out by the good agreement with the available experimental data (9).

Like the finite difference model in this work, models of sensitization applied by Tedmon et al. (8) and Hall and Briant (9) are based on the collector plate concept. The major improvement of these two models over the Stawstrom-Hillert model was the prediction of Cr concentration profiles in the boundary between carbide particles. The shortcoming of both these models, however, is that the concentration profiles between neighboring grain boundary carbides were not permitted to overlap. Thus, midway between the carbide precipitates, the grain boundary Cr concentration was fixed to the initial bulk level. While these models are representative of the very initial stage of sensitization, they cannot describe the condition where an entire boundary will be depleted to less than 13 at % Cr. Nevertheless, during the initial stage of sensitization, the behavior of the finite difference model parallels that of these two limited analytical approaches.

Conclusions

1. The electron backscattering (EBS) technique is both a powerful and easily implemented method for accurately determining the crystallographic orientation and crystal structure of small samples.

2. Grain boundary structures of higher energy sensitize more readily and extensively, and are more corroded in both austenitic and ferritic stainless steels.

3. For ferritic stainless steel, grain boundary corrosion is low for misorientation angles below 10°.

4. A phenomenologically based finite difference model of the "collector plate" mechanism of grain boundary precipitate growth has been successfully developed and used to predict chromium concentration profiles that agree well with experimentally determined profiles. The model avoids certain limitations of existing models and has the capability of being applied in all situations (short, intermediate and long term). It also indicates in what situations existing analytical models can correctly be applied.

5. The model has been successful in treating for the first time the transient period when grain boundary chromium profiles overlap in the boundary.

6. The model relates aging time, temperature and grain boundary structure to sensitization times. Conversely, having Cr profiles in and normal to the grain boundary, carbide spacing or diffusion coefficients can be calculated.

7. Measured Cr depletion zones are much narrower than grain boundary groove widths. This suggests a corrosion mechanism that involves more than the simple dissolution of the Cr depleted regions.

Acknowledgement

The authors thank W. R. Bitler for helpful discussions, H. Shih and M. High for assistance in programming the finite difference model, and R. Iyer and R. Miller for help in preparing the manuscript. Financial support of the Office of Naval Research under Contract No. N00014-84-k-0201 is gratefully acknowledged.

References

1. Bennett, B. W., An Investigation of Intergranular Corrosion of Stainless Steels, Ph.D. Thesis, The Pennsylvania State University (1984).
2. Burgers, J. M., "Geometrical Considerations Concerning the Structural Irregularities to be Assumed in a Crystal", Proc. Phys. Soc., 52 (1940) pp. 23-33.
3. Bragg, W. L., Discussion to Ref. 2, Proc. Phys. Soc., 52 (1940) pp. 54-55.
4. Shockley, W. and Read, W. T., "Dislocation Models of Crystal Grain Boundaries", Phys. Rev., 78 (1950) pp. 275-289.
5. Bollman, W., Crystal Defects and Crystalline Interfaces, Springer-Verlag, New York, NY, 1970.
6. Vitek, V., Sutton, A. P., Smith, D. A. and Pond, R. C., "Atomistic Studies of Grain Boundaries and Grain Boundary Dislocations", pp. 115-148 in Grain Boundary Structure and Kinetics, American Society for Metals, Metals Park, Ohio, 1979.
7. Stawstrom, C. and Hillert, M., "An Improved Depleted-Zone Theory of Intergranular Corrosion of 18-8 Stainless Steel", J. Iron Steel Inst., 207 (1969) pp. 77-85.
8. Tedmon, C. S., Vermilyea, D. A., and Rosolowski, J. H., "Intergranular Corrosion of Austenitic Stainless Steels", J. Electrochem. Soc. 118 (1971) pp. 192-202.

9. Hall, E. L. and Briant, C. L., "Chromium Depletion in the Vicinity of Carbides in Sensitized Austenitic Stainless Steels", Metallurgical Trans., 15A (1984) pp. 793-811.
10. Sakurai, T., Jimbo, A. and Pickering, H. W., "In-Situ Formation of a Grain Boundary in Field Ion Microscopy Using a Laser", pp. 107-109 in 30th Intern. Field Emission Symposium, Univ. Pennsylvania, Philadelphia, PA, 1983: ibid, Applied Physics Letters, submitted for publication.
11. Meibom, R. von and Rupp, E., Z. Phys., 82 (1933) pp. 690-.
12. Boersch, H., Z. Tech. Phys., 18 (1937) pp. 574-.
13. Venables, J. A. and Harland, C. J., "Electron Back-scattering Patterns - A New Technique for Obtaining Crystallographic Information in the Scanning Electron Microscope", Phil. Mag., Ser. A. 27 (1973) pp. 1193-1200.
14. Bennett, B. W. and Pickering, H. W., "A Scanning Electron Microscope Stage for Crystal Orientation and Structure Determination", Scripta Metallurgica, 18 (1984) pp. 743-748.
15. Grimmer, H., "Disorientations and Coincidence Rotations for Cubic Lattices", Acta Cryst., A30 (1974) pp. 685-688.
16. Aaron, H. B. and Aaronson, H. I., "Growth of Grain Boundary Precipitates in Al-4% Cu by Interfacial Diffusion", Acta Metall., 16 (1968) pp. 789-798.
17. Ebling, H. F. and Scheil, M. A., "Time-Temperature-Sensitization (TTS) Diagrams for Types 347, 304L and 316L Stainless Steels", pp. 275-282 in ASTM Spec. Tech. Pub. No. 369, Amer. Soc. Testing and Materials, Philadelphia, PA 1965.
18. Huntz, A. M., Aucoutier, M., and Lacombe, P., "Measure des coefficients de diffusion en volume et intergranulaire du chrome radioactif dans le fer α", Compt. Rend. (Paris), C265 (1957) pp. 554-557.
19. Singhal, L. K. and Martin, J. W., "The Growth of $M_{23}C_6$ Carbide on Grain Boundaries in an Austenitic Stainless Steel", Trans. AIME, 242 (1968) pp. 814-819.
20. Smithells Metals Reference Book, 6th Edition, E. A. Brandes, ed., E. A. Butterworths, London, 1983.
21. Hodges, R., "Intergranular Corrosion in High Purity Ferritic Stainless Steel: Effect of Cooling Rate and Alloy Composition", Corrosion, 27 (1971) pp. 119-127.
22. Briant, C. L., "The Effects of Sulfur and Phosphorus on the Intergranular Corrosion of 304 Stainless Steel", Corrosion, 36 (1980) pp. 497-509.
23. Streicher, M. A., "General and Intergranular Corrosion of Austenitic Stainless Steels in Acids", J. Electrochem. Soc., 106 (1959) pp. 161-180.

SUPPLEMENTARY DISTRIBUTION LIST

Technical and Summary Reports

Dr. T. R. Beck
Electrochemical Technology Corporation
31st Avenue, NE
Seattle, Washington 98125

Professor I. M. Bernstein
Carnegie-Mellon University
Schenley Park
Pittsburgh, Pennsylvania 15213

Professor H. K. Birnbaum
University of Illinois
Department of Metallurgy
Urbania, Illinois 61801

Dr. Otto Buck
Rockwell International
1049 Camino Dos Rios
P.O. Box 1085
Thousand Oaks, California 91360

Dr. W. Morris
Rockwell International
1049 Camino Dos Rios
P.O. Box 1085
Thousand Oaks, California 91360

Dr. David L. Davidson
Southwest Research Institute
8500 Culebra Road
P.O. Drawer 28510
San Antonio, Texas 78284

Dr. D. J. Duquette
Department of Metallurgical Engineering
Rennsselaer Polytechnic Institute
Troy, New York 12181

Professor R. T. Foley
The American University
Department of Chemistry
Washington, D. C. 20016

Dr. J. A. S. Green
Martin Marietta Corporation
1450 South Rolling Road
Baltimore, Maryland 21227

Professor R. H. Heidersbach
University of Rhode Island
Department of Ocean Engineering
Kingston, Rhode Island 02881

Professor H. Herman
State University of New York
Material Sciences Division
Stony Brook, New York 11790

Professor J. P. Hirth
Ohio State University
Metallurgical Engineering
1314 Kinnear Road
Columbus, Ohio 43212

Professor R. M. Latanision
Massachusetts Institute of Technology
77 Massachusetts Avenue
Room E19-702
Cambridge, Massachusetts 02139

Dr. F. Mansfeld
Rockwell International Science Center
1049 Camino Dos Rios
P.O. Box 1085
Thousand Oaks, California 91360

Dr. Jeff Perkins
Naval Postgraduate School
Monterey, California 93940

Dr. E. A. Starke, Jr.
Georgia Institute of Technology
School of Chemical Engineering
Atlanta, Georgia 30332

Dr. R. P. Wei
Lehigh University
Institute for Fracture and
Solid Mechanics
Bethlehem, PA 18015

SUPPLEMENTARY DISTRIBUTION LIST (continued)

Professor H. G. F. Wilsdorf
University of Virginia
Department of Materials Science
Charlottesville, Virginia 22903

Dr. Clive Clayton
State University of New York
Material Sciences Division
Stony Brook, New York 11970

Dr. Henry Leidheiser
Center for Surface and Coatings Research
Sinclair Memorial Laboratory 7
Lehigh University
Bethlehem, PA 18015

Prof. Morris E. Fine
Northwestern University
The Technological Institute
Evanston, IL 60201

Dr. C. S. Kortovich
TRW, Inc.
2355 Euclid Avenue
Cleveland, OH 44117

The Johns Hopkins University
Department of Materials Science & Eng.
Baltimore, MD 21218

Dr. Barry C. Syrett
Stanford Research Institute
333 Ravenswood Avenue
Menlo Park, CA 94025

Prof. S. Weissmann
Rutgers, The State University
of New Jersey
College of Engineering
New Brunswick, NJ 08903

Dr. R. J. Arsenault
University of Maryland
College Park, MD 20742

Prof. A. J. Ardell
University of California
School of Engineering & Applied Science
405 Hilgard Ave.
Los Angeles, CA 90024

Prof. J. G. Byrne
The University of Utah
Dept. of Materials Science & Engineering
Salt Lak City, Utah 84112

Prof. Alexander M. Cruickshank
Gordon Research Conference
Pastore Chemical Laboratory
University of Rhode Island
Kingston, RI 02881

Dr. Paul Gordon
Illinois Institute of Technology
Department of Metallurgical and Materials
Engineering
Chicago, IL 60616

Dr. J. V. McArdell
University of Maryland
College Park, MD 20742

Dr. E. McCafferty
Naval Research Laboratory
Washington, DC 20375

Prof. G. H. Meier & F. S. Pettit
University of Pittsburgh
Dept. of Metallurgical and Materials
Engineering
Pittsburgh, PA 15261

BASIC DISTRIBUTION LIST

Technical and Summary Reports November 1979

Organization	Copies
Defense Documentation Center Cameron Station Alexandria, VA 22314	12
Office of Naval Research Department of the Navy 800 N. Quincy Street Arlington, VA 22217 ATTN: Code 471	1
Code 470	1
Commanding Officer Office of Naval Research Branch Office Building 114, Section D 666 Summer Street Boston, MA 02210	1
Commanding Officer Office of Naval Research Branch Office 536 South Clark Street Chicago, IL 60605	1
Naval Research Laboratory Washington, DC 20375 ATTN: Codes 6000	1
6100	1
6300	1
2627	1
Naval Air Development Center Code 606 Warminster, PA 18974 ATTN: Dr. J. Deluccia	1
Naval Air Propulsion Test Center Trenton, NJ 08628 ATTN: Library	1
Naval Construction Batallion Civil Engineering Laboratory Port Hueneme, CA 93043 ATTN: Materials Division	1
Naval Electronics Laboratory San Diego, CA 92152 ATTN: Electron Materials Sciences Division	1
Naval Missile Center Materials Consultant Code 3312-1 Point Mugu, CA 92041	1
Commanding Officer Naval Surface Weapons Center White Oak Laboratory Silver Spring, MD 20910 ATTN: Library	1
Commander David W. Taylor Naval Ship Research and Development Center Bethesda, MD 20084	1
Naval Oceans Systems Center San Diego, CA 92132 ATTN: Library	1
Naval Underwater System Center Newport, RI 02840 ATTN: Library	1
Naval Postgraduate School Monterey, CA 93940 ATTN: Mechanical Engineering Department	1
Naval Weapons Center China Lake, CA 93555 ATTN: Library	1

total = 87

Organization	Copies
Naval Air Systems Command Washington, DC 20360 ATTN: Codes 52031	1
52032	1
Naval Sea System Command Washington, DC 20362 ATTN: Code 05R	1
Naval Facilities Engineering Command Alexandria, VA 22331 ATTN: Code 03	1
Scientific Advisor Commandant of the Marine Corps Washington, DC 20380 ATTN: Code AX	1
Army Research Office P.O. Box 12211 Triangle Park, NC 27709 ATTN: Metallurgy & Ceramics Program	1
Army Materials and Mechanics Research Center Watertown, MA 02172 ATTN: Research Programs Office	1
Air Force Office of Scientific Research/NE Building 410 Bolling Air Force Base Washington, DC 20332 ATTN: Chemical Science Directorate	1
Electronics & Materials Sciences Directorate	1
AFWAL/MLL Wright-Patterson AFB Dayton, OH 45433	1
Library Building 50, Room 134 Lawrence Radiation Laboratory Berkeley, CA 94700	1
NASA Headquarters Washington, DC 20546 ATTN: Code RRM	1

Organization	Copies
NASA Lewis Research Center Lewis Research Center 21000 Brookpark Road Cleveland, OH 44135 ATTN: Library	1
National Bureau of Standards Washington, DC 20234 ATTN: Metals Sicence and Standards Division	1
Ceramics Glass and Solid State Science Division	1
Fracture and Deformation Division	1
Director Applied Physics Laboratory University of Washington 1013 Northeast Forthieth Street Seattle, WA 98105	1
Defense Metals and Ceramics Information Center Battelle Memorial Institute 505 King Avenue Columbus, OH 43201	1
Metals and Ceramics Divison Oak Ridge National Laboratory P.O. Box X Oak Ridge, TN 37380	1
Los Alamos Scientific Laboratory P.O. Box 1663 Los Alamos, NM 87544 ATTN: Report Librarian	1
Argonne National Laboratory Metallurgy Division P.O. Box 229 Lemont, IL 60439	1
Brookhaven National Laboratory Technical Information Division Upton, Long Island New York 11973 ATTN: Research Library	1
Office of Naval Research Branch Office 1030 East Green Street Pasadena, CA 91106	1

END

FILMED

9-85

DTIC